Journal of Chromatography, 588 (1991) 239–249
Elsevier Science Publishers B.V., Amsterdam

CHROM. 23 645

Photoemissive ionisation source for ion mobility detectors

P. Begley, R. Corbin, B. E. Foulger* and P. G. Simmonds

Admiralty Research Establishment, Holton Heath, Poole, Dorset BH16 6JU (UK)

(First received April 17th, 1991; revised manuscript received July 19th, 1991)

ABSTRACT

A combination of a photoemissive ionisation source coupled to an ion mobility detector has been developed which utilises a pulsed light source thereby eliminating the need for an ion injection gate. Factors influencing the performance of this negative ion detector have been investigated. With air as the sample and drift gas streams, the performance of the detector is comparable to conventional designs employing radioactive ionisers.

INTRODUCTION

Recently, there has been renewed interest in the ion mobility spectrometer [1], both as a stand-alone detector [2–9] and as a detector for use with a range of separation techniques including gas chromatography [10–14], supercritical fluid chromatography [15,16], high-performance liquid chromatography [17], and capillary electrophoresis [18]. In a conventional ion mobility spectrometer, ionisation is produced using a ^{63}Ni radioactive foil, which emits a steady current of electrons of energies up to 67 keV [19]. As alternatives to radioactive ionisation, other workers have used photoionisation [20–23], non-resonant laser photoionisation [24], resonant two-photon laser ionisation [25,26], corona [27], and coronaspray ionisation [28]. The work presented here has concentrated on the investigation of a photoemissive source based on ultraviolet irradiation of a thin gold layer with a work function of *ca.* 4.5 eV [29]. This photoemissive source has several potential advantages. Firstly, it is unipolar, generating an initial population of only gaseous low-energy electrons, so eliminating possible loss mechanisms involving both positive ion–negative ion or positive ion–electron recombination. Secondly, it is free from constraints associated with the safe handling of radioactive materials, and thirdly, the initial electron concentration can be controlled, in principle, over a wide range simply by changing the incident light intensity. Furthermore, when combined with a pulsed light source it offers the attractive design option of eliminating the shutter grid at the entrance to the drift tube and its associated gating electronics, so reducing signal losses. Photoemission electron sources have been used in low-pressure drift tubes [30–35], in negative ion detectors [36–40] and as a source of thermal electrons in an electron-capture detector [41,42]. The combination of a photoemissive source with an ion mobility spectrometer as described in this paper is, to our knowledge, the first practical demonstration of such a device for trace analysis at atmospheric pressure.

EXPERIMENTAL

The design of the detector is shown in Fig. 1. The drift tube (Welwyn Electronics, Bedlington, UK) is composed of a 10 mm I.D. × 12 mm O.D. ceramic cylinder which has been internally coated with a low-conductivity ink to produce a nominally uniform resistance of *ca.* 2 MΩ cm^{-1}, whilst a high-conductivity ink was applied to the ends to facilitate electrical connections. The tubes used were 3.7 cm long, but by selecting a well matched pair (8.0 ± 0.1 MΩ),

0021-9673/91/$03.50

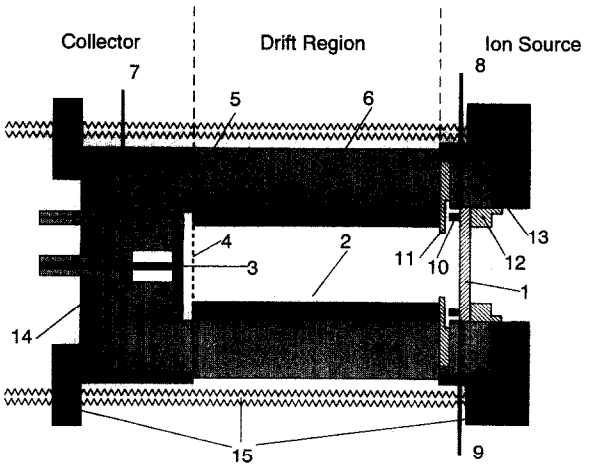

Fig. 1. Photoemissive ion mobility cell. Key: 1 = gold-coated photoemissive window; 2 = drift tube; 3 = perforated collector; 4 = screen grid; 5 = annular guard electrode; 6 = PTFE body; 7 = drift gas inlet; 8 = sample gas inlet; 9 = exhaust gas outlet; 10 = graphite "O"-ring; 11 = gas access plate; 12 = threaded vespel plug; 13, 14 = brass end caps; 15 = clamping (× 3).

two tubes could be used in tandem to give a drift length of 7.4 cm with correspondingly increased ion resolution. In the work reported here, both 3.7 cm and 7.4 cm drift lengths were evaluated experimentally. The photoemissive window was produced by placing 11 mm O.D. × 1.5 mm thick high-purity fused-silica discs (TSL Group, Wallsend, UK) in a sputter coater (Model S150B; Edwards High Vacuum, Crawley, UK), followed by coating with gold for *ca.* 2 min. The performance of the photoemitters was found to be only slightly dependent on the sputter coating time over the range 45 s to 2.5 min. Once the window is assembled in the detector the effective photoemissive window diameter is 9 mm. The screen grid was purchased from Graseby Ionics (Watford, UK) and consisted of a gold-plate photoetched mesh, mounted upon a ceramic former. As the detector was operated with a drift voltage of *ca.* 2000 V on the collector, a guard ring held at the same potential as the collector was incorporated to reduce leakage currents. This configuration whereby the collector is operated at high potential, as opposed to the more conventional arrangement with the collector grounded, was adopted to facilitate studies in which fields within the ion source field could be pulsed. The machining of the various detector components was carried out without the use of cutting fluids to minimise problems arising from contamination.

The signal from the collector was taken to an optically isolated voltage-to-current convertor and head amplifier, which was designed and manufactured in-house, and was mounted within a screened enclosure attached to the drift tube assembly. The main drift field (*ca.* 240 V cm^{-1}) was supplied from an EMI PM28B photomultiplier power supply, which was also used as the current source for high-voltage operation of the detector electronics. A second power supply was developed in-house to supply the lens polarising voltage. This power supply also contained appropriate driver circuitry to allow it to be used with a gating grid.

For the majority of this work, a pulsed xenon lamp (Hamamatsu, type L2415 or L2439) with its associated power supply (Hamamatsu, type C2190-01) was used as the illumination source. The pulse repetition rate was operated as high as possible while still ensuring that the product ions from each flash reached the detector before the next flash. This corresponded to a repetition rate of *ca.* 50 Hz for the short tube, and *ca.* 30 Hz for the long tube. A series of experiments were also conducted with continuous output low-pressure mercury lamps ("Pen-Ray" Ultra-Violet Products, San Gabriel, CA, USA) operated in a pulsed mode using a laboratory constructed pulsed power supply driven by a Hewlett-Packard Model 214B pulse generator.

The signal from the detector amplifier was displayed on a Nicolet Model 4094A digital storage oscilloscope which allowed signal averaging, integration, etc., to be undertaken. To study the effect of different wavelengths of incident light, measurements were carried out using an Oriel Model 7185 photodiode and a Nicolet 430E digital storage oscilloscope. The latter had a higher sampling rate than the 4094A oscilloscope and so was more appropriate for monitoring the light pulses of width at half height of *ca.* 10 μs. A Spectral Energy GM100-3 monochromator was used with 1 mm entrance and exit slit widths in conjunction with the Hamamatsu lamps to provide monochromatic illumination. The results were not corrected for variation in the spectral response of the photodiode since the response variation was minimal over the wavelength range studied. The VU-POINT software

package (S-CUBED; Maxwell Labs., La Jolla, CA, USA) was used to transfer data stored on the Nicolet 4094A's discs directly into an IBM PC-compatible computer.

In operation, a high drift gas flow was maintained through the inlet in the collector region, while the sample gas flow entered through one of two ports in the ion source, the other port forming the exhaust. Drift gas, either air, or for some experiments, "oxygen-free" [< 8 vpm (ppm, v/v) oxygen] nitrogen, was supplied through two stage regulators (Model 11 or 11A; Scott Environmental Technology, Plumsteadville, PA, USA) fitted with stainless-steel diaphragms and passed through a trap containing a mixture of charcoal, 5A and 13X molecular sieves to precision gas-pressure regulators (Porter Model 8286) fitted with stainless-steel bodies and diaphragms. Gas flows were controlled by needle valves (Nupro Model SS-SS1) and were measured using digital mass flowmeters (Teledyne-Hastings-Raydist). To perform quantitative measurements, a simple gas manifold was built which allowed compounds of known vapour pressure to be continuously diluted in one or two stages with dry air to a known concentration, which could then be admitted to the detector for long periods. A gas blender (Model 850; Signal Instrument Co., Camberly, UK) was used in experiments in which the oxygen content of both drift and sample gas streams was varied in the range 0 to 20% (v/v). In normal operation, 50–100 ml/min of gas was maintained through the sample inlet port with a drift gas flow of 250–300 ml/min. The system was operated at ambient temperature and pressure for all experiments. In some experiments, the sample inlet was sealed off and a flow of 300–400 ml/min of gas, which included a target chemical at a known concentration, was admitted through the drift gas inlet. When not in use, a small purge gas flow of 10–20 ml/min was always maintained through the detector.

RESULTS AND DISCUSSION

Initially a series of experiments were conducted to investigate the influence of a number of design aspects on the detector performance, which was assessed by measuring the size and width of the $O_2^-(H_2O)_n$ reactant ion peak. Two methods of illuminating the ioniser were evaluated. In the first method, a xenon flashlamp with fixed pulse length but adjustable intensity was used. For comparison, a low-pressure mercury lamp was operated at constant intensity but with variable pulse length. Unfortunately the design of this lamp did not permit any variation in the intensity. It was found that the light output from the mercury lamp was disproportionately low at short pulse lengths as the lamp was not reaching its correct operating temperature resulting in the mercury vapour pressure within the lamp not being sufficiently high. This was corrected by wrapping the bulb in heating wire and maintaining the outside of the silica envelope at a temperature of *ca.* 75°C. With this system, the total light input was controlled by varying the pulse width. Fig. 2 compares the reactant ion characteristic across the accessible range of light intensities for this light source and the xenon lamp for a 3.7 cm drift cell. In this and subsequent figures, resolution has been defined as the drift time divided by the peak width at half height. Clearly the major drawback with the mercury lamp is its low output, leading to unacceptable losses in resolution when the pulse width was increased to give an acceptable signal size. However, the variable pulse width from the mercury lamp did allow the experimental resolution to be compared with values calculated from Spangler and Collins' theoretical derivation [43] by substituting the lamp pulse length for the gate width. Although Fig. 3 shows the experimental data qualitatively followed

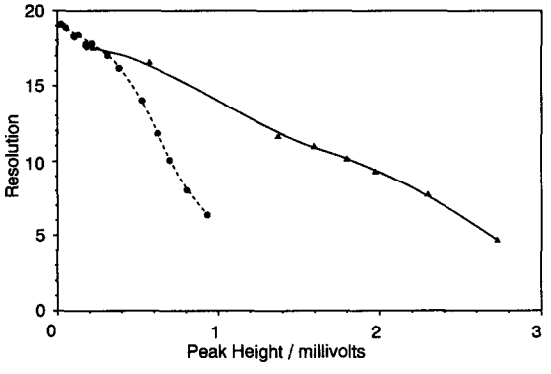

Fig. 2. Effect of the light source on the detector performance. Circles: illuminated by low-pressure mercury lamp. Triangles: illuminated by xenon flash lamp. Conditions: 3.7 cm drift tube, 920 V drift field, photoemissive lens 80 V, sample flow 50 ml/min, drift flow 300 ml/min, temperature 292–297 K.

the theory, the experiments yielded resolutions which are consistently lower than those predicted. The variation in peak height with lamp pulse width is also shown in Fig. 3. No variation was observed in the baseline noise as the pulse width was altered, and signal to noise ratios would have been proportional to the peak heights.

The subsequent study of the effect of the illumination wavelength, as shown in Fig. 4, indicates that illumination at 254 nm, which constitutes the bulk of the output from the mercury lamp, is relatively inefficient. In Fig. 4, the efficiency is defined as the detector output per unit intensity input relative to 220 nm. In contrast, the xenon lamp has strong emission lines in the 200–250 nm region, and its overall output power is also much greater. The emission spectrum measured here is in good qualitative agreement with results previously reported for similar lamps [44]. As a result, the xenon lamp was adopted as the preferred light source for this study.

A series of photoemissive windows were prepared using masks of different diameters and exposing the windows to extended sputter coating times of 5 min. This produced a series of windows with a opaque conductive outer rim and a central transparent region. After removal of the mask, each window was then coated for 2 min to the usual density. These windows were then installed in turn in a 7.4 cm drift length detector, and the peak widths, heights and areas measured for the oxygen reactant ion peak as

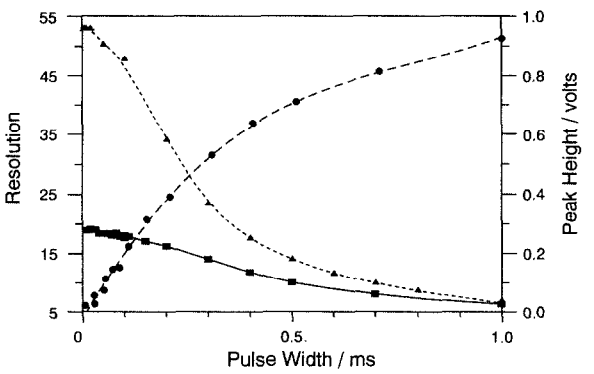

Fig. 3. Comparison of the calculated and experimental resolution for a 3.7 cm drift tube. Triangles: theoretical resolution values. Squares: experimental resolution values. Circles: experimental peak heights. Conditions as in Fig. 2.

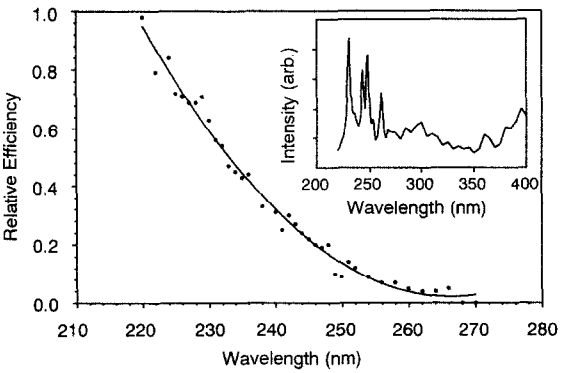

Fig. 4. Relative photoemission efficiency as a function of wavelength. Inset: emission spectrum of the xenon flash lamp.

the input light intensity was varied. The results of these experiments are summarised in Fig. 5. Several aspects of this work are of relevance to future designs. Firstly, the resolution increases as the window area decreases, which presumably reflects the greater uniformity of the drift field near the centre of the tube. However, the resolution of the

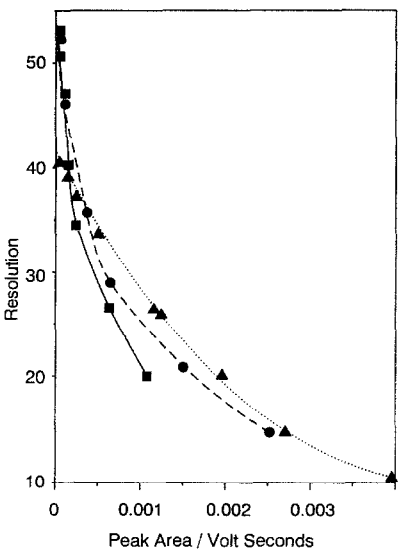

Fig. 5. Effect of the photoemissive window diameter on the detector's performance. Solid line: 2 mm diameter. Dashed line: 3 mm diameter. Dotted line: 9 mm diameter. Conditions: 7.4 cm drift tube, 1900 V drift field, photoemissive lens 80 V, sample flow 70 ml/min, drift flow 260 ml/min, temperature 292–297 K.

smaller windows degrades much more rapidly as the peak area increases than does that for the larger window diameters. This strongly suggests that mutual ion repulsion is a significant factor at the ion densities generated and any attempt to improve the detector's sensitivity by further increasing the input light intensity, and hence the reactant ion density, would be counter-productive, as the increased yield of ions would be offset by degraded resolution. A better approach, which will be the subject of future research, is to design detectors which operate at similar light intensities to those currently used, but with a larger tube diameter and greater active photoemissive area.

There are several factors that contribute to the observed resolution for gridless systems that are not relevant with a conventional gated source. In the gated source, processes occurring in front of the entrance gate do not contribute to the observed resolution, which is determined by the shape and duration of the gate pulse, diffusional broadening, ion molecule reactions within the drift tube and other factors which have been identified by previous workers in the field [45]. All of these factors are also present in the gridless system but in addition, resolution can also be affected by processes occurring within the ionisation region. In addition to mutual ion repulsion described above, any steps occurring within the ionisation region on timescales comparable with the peak widths could degrade the resolution. Clearly, as shown in Fig. 3, the lamp pulse width can affect the resolution. However, the xenon lamp used in the majority of our studies has a pulse half-width of only 0.01 ms which will not significantly increase the ion peak width. Also, the finite distance the electrons travel prior to conversion to O_2^- reactant ions must be considered. Using a three-body attachment rate constant of $2 \cdot 10^{-30}$ cm^6 s^{-1} at *ca.* 290–300 K for the reaction $e^- + O_2 + M \rightarrow O_2^- + M$ (where $M = O_2$) [46], the electrons will have a lifetime in air of *ca.* $2 \cdot 10^{-8}$ s. Since, at room temperature, the rate constant for the reverse reaction is negligible and the three-body rate constant for O_2^- formation with nitrogen as the third body is at least an order of magnitude less [46], the contribution of these two processes to the lifetime of the electron in air have been ignored. At a E/N value of *ca.* 10^{-17} V cm^2 the drift velocities of electrons in nitrogen and oxygen at 293 K are $5 \cdot 10^5$ and 10^6 cm s^{-1}, respectively [47] (E is the electric field intensity and N the gas number density, and their ratio is commonly used to characterise the average energy which an ion acquires from an applied electric field). Therefore, assuming an electron drift velocity in air of *ca.* $6 \cdot 10^5$ cm s^{-1}, the electrons will only penetrate *ca.* $1.2 \cdot 10^{-2}$ cm along drift tube prior to conversion to O_2^- reactant ion. For a reactant ion drift velocity of *ca.* $5 \cdot 10^2$ cm s^{-1}, this means the half peak width of the reactant ion peak will be increased by *ca.* 0.02 ms as a result of the electron drift in air. The observed half peak widths at the lowest light levels are 0.34 ms for our standard photoemissive window. Therefore, the electron drift in air is not an important factor in determining the system resolution. However, this argument is only valid at low electron concentrations since, as we have observed, mutual charge repulsion will degrade resolution at higher concentrations of electrons or ions. In practice (see later) the most important processes are the sequence of ion molecule reactions leading to the observed product ions.

In order to direct the design changes within the photoemissive source into potentially useful areas, a series of kinetic model simulations were made using rate constants from the literature, and concentrations equivalent to those encountered in testing the prototype gridless detectors. The primary motivation was to derive information about the timescales required for the product formation reaction, and to compare these with the detectors' characteristics. For this purpose, the model was constructed to simulate reactions occurring in a closed, homogeneous gas mixture in the absence of applied electric fields. In this way, the equilibration times required for the reactions could be determined, and compared with the species lifetimes implied by the detector designs. The simulations were implemented using the simulation program CHEKMAT (AERE, Harwell, UK) [48] which is specifically designed to produce numerical solutions to problems involving systems of chemical reactions and simultaneous diffusion, although the latter capability was not required in this case. A series of runs were made, simulating the following system of reactions, where P represents the target compound:

$$e^- + O_2 \rightarrow O_2^-$$

$$O_2^- + P \rightarrow P^- + O_2$$

$$P^- \rightarrow P + e^-$$

Although the equations above imply charge transfer from the oxygen ion, attachment of the oxygen ion to form an adduct, or second order nucleophilic substitution, is mathematically equivalent, and so conclusions about reaction timescales can be applied to any of these reaction mechanisms. The oxygen concentration was that derived assuming standard temperature, pressure and composition. The concentration of the target compound P was assumed to be 70 ppb[a] at standard temperature and pressure in most cases, but was varied to 7 ppb for a few comparative runs. The number of electrons was measured directly on the gridless photoemission cell with nitrogen drift gas using a Kiethley Model 617 electrometer connected to the collector, and light intensities identical to those used in normal operation. No correction was applied for losses to the wall of the drift tube. By measuring peak widths on the oxygen ion, a maximum reaction volume was derived ignoring the effect of diffusional broadening, and so tending to overestimate the volume. The electron concentration was then calculated assuming that it was homogeneous throughout this volume.

The electron attachment to oxygen was modelled using the treatment developed by Shimamori and Hatano [49], which uses a Bloch–Bradbury mechanism, modified for the effect of third-body stabilisation, by both oxygen and nitrogen, using measured rate constants [50–52] from the literature. The lifetime of the oxygen ion was taken as that measured by Shimamori and Hatano, which is in reasonable agreement with theoretical calculations [53,54]. In accordance with the rate constants measured by workers using flowing afterglow techniques, a range of values were assumed for charge transfer from, or attachment of, the oxygen anion, covering the values found for fast reactions (10^{-10} – $3 \cdot 10^{-9}$ cm^3 molecule^{-1} s^{-1}). No measured rate constants for the decay or further reaction of the product anions have been found in the literature. Autodetachment lifetimes, which are the lifetimes of the excited ions formed by capture of a free electron, have been measured for perfluorotoluene and perfluoromethylcyclohexane [55], so simulation runs have been made covering the range of possible autodetachment rates implied by these lifetimes. The rate of consumption of the product ion implied by these lifetimes is equivalent to that which would be observed if it was consumed in a second-order process proceeding at the collision limit with a second species present at 15–100 ppb levels. Fig. 6 shows some typical results.

A wide range of simulation runs were conducted covering the range of conditions described above. By eliminating the reactions of the target compound P, and modelling only the capture of electrons by oxygen, good agreement was found with the calculations of Grimsrud and Stebbins [56] after allowing for differences in concentrations. The following salient conclusions can be made from our simulations:

(a) While the electron transfer reaction to oxygen was extremely fast (10–100 ns), equilibration times for the target compound P ion formation were much longer (10–1000 μs). The free electron concentration was negligible within a period of 1 μs.

(b) The equilibration time was critically dependent upon the lifetime of the product ion. In the case of perfluorotoluene the system reaches equilibrium within 40 μs, whilst for an extremely long-lived ion such as perfluoromethylcyclohexane, significant further product formation is continuing even after 1 ms.

(c) For a given reaction time, the number of product ions formed increases as the postulated lifetime increases.

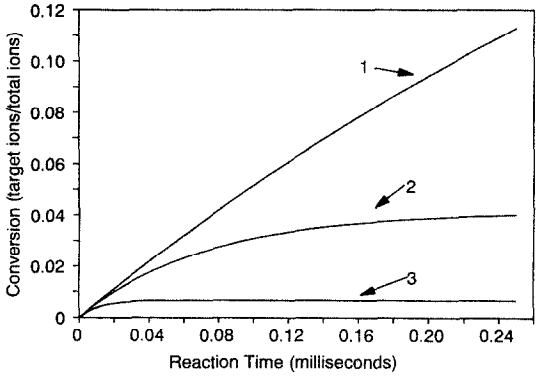

Fig. 6. Simulation runs for a formation rate of $3.0 \cdot 10^{-10}$ cm^3 molecule^{-1} s^{-1} and decay rates of (1) $1.3 \cdot 10^3$ s^{-1}, (2) $1.3 \cdot 10^4$ s^{-1} and (3) $8.3 \cdot 10^4$ s^{-1}.

[a] Throughout this article, the American billion (10^9) is meant.

(d) The formation rate has a direct influence on the number of ions after a given reaction time, but has no apparent effect upon the equilibration time.

(e) When direct electron capture by the target compound P was included in the simulation using a rate constant typical of perfluorocarbons, there was a significant increase in the initial rate of product formation, but this was rapidly dwarfed by the contribution through charge transfer, and was an insignificant contribution to the total at reaction times greater than 25 μs.

(f) Simulations at concentrations of target compound P of 70 ppb and 7 ppb showed no difference in equilibration time, but there appeared to be a small increase in overall ionisation efficiency at 7 ppb. If this accurately reflects the real behaviour, then departure from a linear concentration/signal relationship will occur at 70 ppb levels.

In the context of detector design, the most relevant aspect of these simulations was the prediction of reaction times of the order of milliseconds for optimal product ion yield, and hence sensitivity. Since the gridless photoemission detector was estimated to allow reaction times of no more than 0.2–0.3 ms based on the observed peak widths of the reactant ion, this strongly suggests that improved performance could be achieved if the reaction time could be increased without compromising the detector's resolution.

One advantage which was predicted for the photoemissive devices was that the absence of signal losses through positive ion–negative ion neutralisation reactions would result in improved product ion yields, and hence sensitivities, when compared to the bipolar radioactive source. In order to assess the likely importance of this advantage, the reaction system described above was modified to include positive ions at the same concentration as electrons. These were then permitted to undergo neutralisation reactions with both the reactant oxygen ion and the product anion, with a rate constant of $2.0 \cdot 10^{-6}$ cm^3 ion^{-1} s^{-1}, which is the upper limit suggested by both theoretical and experimental studies [57,58]. Other candidate loss mechanisms such as radiative and dissociative electron-ion recombination have been excluded from consideration since the predicted electron concentration within the source is negligible except at very short times. Fig. 7 demonstrates the effect of these processes on the predicted ion yield, with the equivalent unipolar case included for comparison. The particular set of conditions used in these simulation runs are for a very long-lived product ion at low concentrations. While the absence of recombination pathways is a significant advantage at long reaction times, giving an increased yield by approximately a factor of two, very little advantage (10–20%) is gained over the 0.2–0.3 ms timescales estimated for reaction in the gridless photoemission system. This has provided further motivation for attempts to increase the available reaction time in the photoemission source designs.

A series of determinations were made on the 3.7 cm drift length detector cell in which the oxygen content of both the drift and sample gas streams was varied in the range 0 to 20% (v/v). A further series of experiments was conducted in which the sample gas stream was varied in oxygen composition, while the drift stream was pure nitrogen. These results are presented in Fig. 8. This series of experiments highlights several important features of the gridless photoemissive system. Where oxygen is present in both the sample and drift streams, the resolution is effectively unchanged at oxygen concentrations in excess of 6% (v/v). Furthermore, the resolution declined as the oxygen content decreased, which strongly suggests that electrons were able to travel substantial distances along the drift tube before attachment to oxygen molecules. The peak shapes confirmed this interpretation, as a progressively

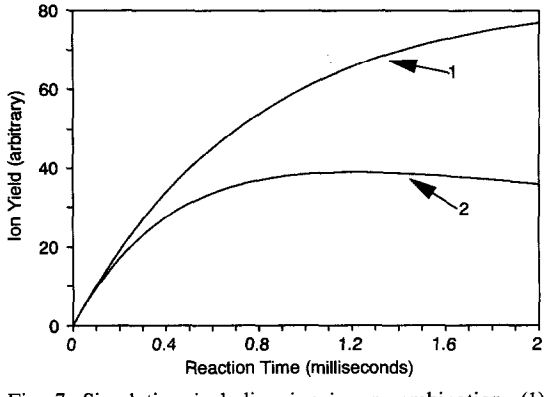

Fig. 7. Simulation including ion–ion recombination. (1) No recombination. (2) Recombination rate of $2.0 \cdot 10^{-6}$ cm^3 molecule^{-1} s^{-1}.

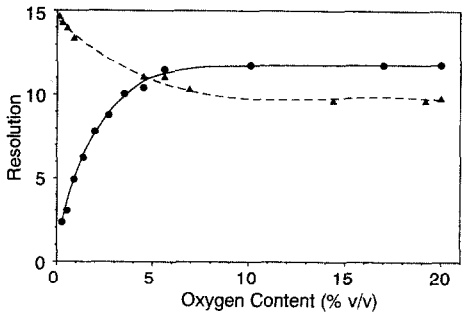

Fig. 8. Effect of the gas composition on the reactant ion resolution. Solid curve: both the sample and drift streams contained the indicated oxygen level. Dashed curve: oxygen was present only in the sample gas stream. The balance was nitrogen in both cases. Conditions as in Fig. 2, except sample flow 45 ml/min, drift flow 220 ml/min.

more conspicuous leading edge "shoulder" developed on the reactant ion as the oxygen content was reduced. For the situation with nitrogen drift gas and where a varying oxygen content is admitted into the sample stream, the peak resolution improves as the oxygen content of the sample gas is reduced. Since the nitrogen drift flow is approximately five times greater than the sample inlet flow this leads to the complication that the effective oxygen concentration in the reaction zone will be reduced by one fifth, assuming complete mixing. Therefore because relatively few oxygen molecules are available for electron attachment, the concentration of oxygen anions will not reach a sufficiently high density for mutual ion repulsion to significantly degrade resolution, while many electrons will simply escape capture altogether. The observation that with oxygen present in the drift gas the overall resolution is greater in the plateau region may be due to the increased rate constant for the electron attachment reaction when oxygen acts as the third body [46]. A smaller reaction volume is associated with this faster rate constant, therefore accounting for the improved resolution.

The detector response was measured for some representative target compounds in each of two flow configurations. In the "conventional flow" configuration, pure drift gas was introduced at the collector inlet on the cell and the gas stream containing the target chemical was introduced at the inlet immediately adjacent to the photoemissive window. In this configuration the bulk of the cell drift volume does not contain the unionised target chemical. For comparison, measurements were also carried out with the sample inlet port sealed off and the target chemical introduced into the drift gas stream, so producing a uniform target chemical concentration throughout the drift volume.

Fig. 9 shows the observed response for concentrations of benzoquinone up to 200 ppb. Furthermore, Fig. 9 illustrates that when the sample is introduced into the drift flow increased sensitivity is observed at the lower concentrations. Similar results were observed for methyl salicylate and 4-chloronitrobenzene. The observed sensitivity enhancement, defined as the ratio of the peak height in the "sample in drift" mode to the peak height in the "conventional flow" mode, and measured at low concentrations, was calculated as 18.7 for benzoquinone, 4.8 for 4-chloronitrobenzene, and 2.9 for methyl salicylate. These response enhancements suggest that in the conventional flow configuration, the oxygen ion reactant peak is not present in a region of significant target neutral concentration for a sufficient time to allow the reaction to reach equilibrium. In the "conventional flow" configuration, the concentration is that which was delivered in the sample gas line, and has not been adjusted for dilution by the drift gas, as it has not proved possible to calculate

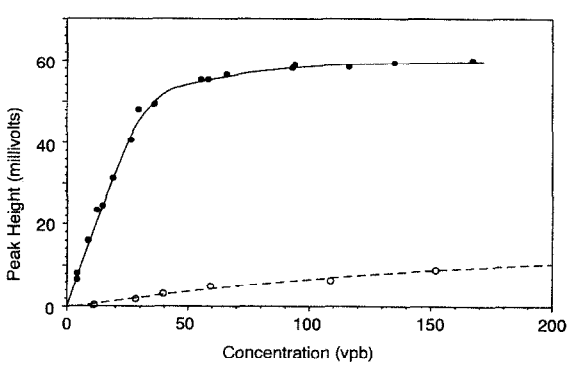

Fig. 9. Response of the detector to benzoquinone (BQ). Dashed curve: "conventional" flow pattern (BQ present only in the sample gas stream). Solid curve: sample inlet blanked off and sample of BQ introduced through the drift gas inlet. Conditions as in Fig. 5, except in "conventional" mode sample flow 50–80 ml/min, drift flow 200–230 ml/min, in "sample in drift" mode, drift flow 280–320 ml/min.

the actual concentration in the reaction zone. It could be argued that the inlet concentration is the more relevant quantity to help assess the detector's applicability in real-world applications. However, this uncertainty in the concentration in the reaction zone makes the comparison of the two flow configurations less clear-cut than we would wish, although the results for benzoquinone cannot be completely explained by a simple dilution effect since for the sample and drift flow-rates used in this work the maximum envisaged relative enhancement would be *ca.* 6, while 18.7 was observed. Such a maximum enhancement could only arise if complete mixing of the sample and drift flows occurred at the sample inlet while in the "conventional flow" configuration, whereas we believe that a more or less well-defined plume of sample gas, which is progressively diluted by the drift gas as the exhaust outlet is approached, is generated across the face of the photoemissive window. In contrast, when the target compound is present throughout the drift region, longer reaction times are available and so the equilibrium distribution is more closely approached. The wide variation in the enhancement ratio for the different compounds is believed to reflect differences in the formation rates and stabilities of the ions formed. Unfortunately, we were unable to find any appropriate kinetic data in the literature to support this view. When the system was operated in the "sample in drift" mode, the product ion peaks were wider than those observed in the "conventional flow" mode, and, at lower concentrations, a leading edge "shoulder" appeared. For benzoquinone at concentrations of *ca.* 15 ppb, the measured resolution was 33 in the conventional flow mode, but only 18 when the sample was introduced in the drift gas. Again this is consistent with the reaction continuing after the oxygen ions had moved a significant distance down the drift tube. As a consequence, the sensitivity enhancement quoted above is not fully realised as an improved limit of detection. In the current experiments, 256 spectra were averaged for each determination, and the detection limits were estimated to lie in the range 0.2–5 ppb. Sensitivities of this order are broadly comparable with those claimed for radioactive ion mobility detectors [59], although the large variation in sensitivity to different chemicals complicates the comparison. A more comprehensive study is currently underway to quantify the limits of detection of the gridless photoemissive and ^{63}Ni radioactive sources on a test assembly in which the source assemblies are interchangeable. As illustrated in Fig. 10, when the system was operated in the conventional flow configuration, the reactant ion peak dominates the ion mobility spectrum. As the target chemicals are reduced in concentration, poor resolution from the reactant ion peak becomes the controlling factor in defining their detection limits. Fig. 8 also demonstrates that the product ion peaks could, for some compounds, achieve higher resolution than did the reactant peak.

A series of experiments were also conducted in which the flash rate of the Hamamatsu lamp was varied while low levels of target chemicals were introduced into the gridless 7.4 cm detector. This was accomplished by disconnecting the trigger signal supplied from the ion mobility electronics, so producing a lamp pulse every 30 ms, and using the lamp power supply's internal trigger, which is variable over the range 10–120 ms. The oscilloscope was synchronised with the flash lamp by monitoring the lamp with an Oriel 7185 photodiode and using the photodiode output as the external trigger for the oscilloscope. In air, in all cases, a precursor to the main reactant peak was found that increased in magnitude as the flash repetition rate was increased. This precursor was observed in other experiments, particularly when a given photoemissive window had been in use for several weeks, and has been tentatively ascribed to O_3^-, on the basis of its relative mobility [60] and since it was found to increase in size if the sample gas stream was subjected to intense

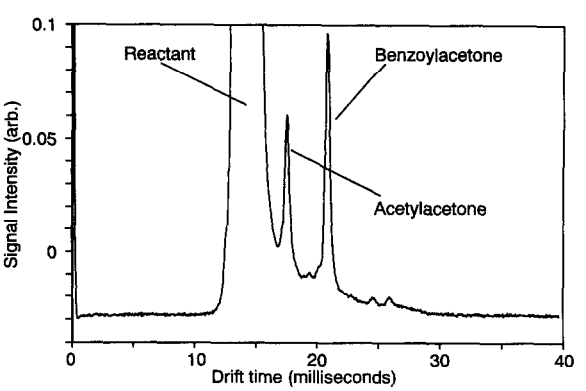

Fig. 10. Ion mobility spectrum for acetylacetone and benzoylacetone at trace levels. On the *y*-axis scale shown, the full height of the reactant peak is *ca.* 1. Conditions as in Fig. 5.

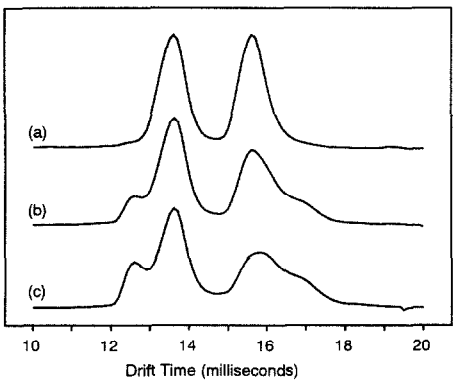

Fig. 11. Effect of the flash repetition rate on the benzoquinone mobility spectrum (reactant peak drift time *ca.* 13.5 ms, BQ product peak drift time *ca.* 15.7 ms). (a) Lamp flashes at 110-ms intervals. (b) Lamp flashed at 22-ms intervals. (c) Lamp flashed at 11-ms intervals. Conditions as in Fig. 5.

short-wave ultraviolet radiation before admission to the detector cell. The principal O_2^- reaction ion peak was observed to decrease in magnitude in an approximate inverse proportion. In the presence of target chemicals such as acetylacetone, methyl salicylate and benzoquinone, the expected product ion peak was reduced in magnitude to a greater degree than the reactant peak, and in the case of benzoquinone a trailing edge shoulder developed on the peak, suggesting that another product ion was being formed. For perfluorodimethyladamantane, the observed effects were much smaller, with no major reduction in product ion intensity accompanying higher flash rates. However, a small trailing edge shoulder which was present on the product ion peak at low repetition rates diminished as the flash rate increased. No conclusive explanation can be offered for this contrasting behaviour, but it may reflect differences in the ionisation mechanisms for the various compounds used. Typical results, in this case for benzoquinone, are summarised in Fig. 11. It was noted that these above effects became more severe if the total flow of gas through the detector was reduced, which suggests that they might be caused by the production of photoexcited neutral species from the target molecule, or by the photochemical production of ozone within the ionisation region. Either of these products, being neutral, would be cleared from the detector only by ventilation in the cell exhaust. This ventilation would be expected to have a half lifetime of 5–10 ms and is therefore on a comparable timescale to the flash repetition rate. Once formed such photochemical products could participate in a range of reactions with either the reactant ions or the desired product ions. Such reactions need not lead to the production of observable peaks in the ion mobility spectrum, if the reaction products were unstable with lifetimes less than their drift times. Ideally, these effects should be studied in greater detail using spectroscopic or mass spectral techniques.

CONCLUSIONS

This work has demonstrated that photoemission can be exploited as a viable ionisation technique for use in ion mobility detectors. Several factors have been investigated that influence the performance of a photoemissive ion mobility detector. For the gridless design investigated here, the evidence suggests that the ion–molecule chemistry which leads to the characteristic product ions may not be proceeding to equilibrium under the conditions attainable and that the sensitivity of the detector may be reduced as a result. Further work is now in progress using a photoemissive detector in which a conventional drift tube entrance grid is also employed, so that, by delaying operation of the gating grid with respect to the light pulse, longer reaction times can be tolerated in the ion source without degrading the resolution of the detector in the manner described here. Furthermore the performance of the photoemissive source is currently constrained by mutual ion repulsion degrading the ion resolution and studies are in hand using wider bore systems to reduce the ion densities.

ACKNOWLEDGEMENTS

The authors would like to thank Dr. J. Lovelock for advocating the use of a photoemissive ionisation source and for useful discussions on aspects of this work. We also thank Mr. F. Norris and Mr. P. Hunter for fabrication of the prototype detectors.

REFERENCES

1 H. H. Hill, Jr., W. F. Siems, R. H. St. Louis and D. G. McMinn, *Anal. Chem.*, 62 (1990) 1201A.

2 J. P. Carrico, A. W. Davis, D. N. Campbell, J. E. Roehl, G. R. Sims, G. E. Spangler, K. N. Vora and R. J. White, *Am. Lab.*, 152 (1986) 155.
3 C. J. Proctor and J. F. Todd, *Anal. Chem.*, 56 (1984) 1794.
4 A. H. Lawrence and P. Neudorfl, *Anal. Chem.*, 60 (1988) 104.
5 G. E. Spangler, J. P. Carrico and D. N. Campbell, *J. Test. Eval.*, 13 (1985) 234.
6 S. H. Kim and F. W. Karasek, *Anal. Chem.*, 50 (1977) 152.
7 G. E. Spangler and J. P. Carrico, *Int. J. Mass Spectrom. Ion Phys.*, 52 (1983) 267.
8 G. E. Spangler, K. N. Vora and U. P. Carrico, *J. Phys. E: Sci. Instrum.*, 19 (1986) 191.
9 G. E. Spangler, D. E. Campbell and J. P. Carrico, *US Pat.*, 4 551 624 (1985).
10 F. W. Karasek, H. H. Hill, Jr., S. H. Kim and S. Rokushika, *J. Chromatogr.*, 135 (1977) 329.
11 M. A. Baim and H. H. Hill, Jr., *J. Chromatogr.*, 299 (1984) 309.
12 M. A. Baim and H. H. Hill, Jr., *J. High Resolut. Chromatogr. Chromatogr. Commun.*, 6 (1983) 4.
13 R. H. St. Louis, W. F. Siems and H. H. Hill, Jr., *J. Microcolumn Sep.*, 2 (1990) 138.
14 R. H. St. Louis, W. F. Siems and H. H. Hill, Jr., *J. Chromatogr.*, 479 (1989) 221.
15 H. H. Hill, Jr. and M. A. Morrissey, in C. M. White (Editor), *Modern Supercritical Fluid Chromatography*, Hüthig, Heidelberg, 1988, p. 95.
16 R. L. Eatherton, M. A. Morrissey, W. F. Siems and H. H. Hill, Jr., *J. High Resolut. Chromatogr. Chromatogr. Commun.*, 9 (1986) 154.
17 D. G. McMinn, J. Kinzer, C. B. Shumate, W. F. Siems and H. H. Hill, Jr., *J. Microcolumn Sep.*, 2 (1990) 188.
18 R. W. Hallen, C. B. Shumate, W. F. Siems, T. Tsuda and H. H. Hill, Jr., *J. Chromatogr.*, 480 (1989) 233.
19 F. W. Karasek, *Res. Develop.*, 21 (1970) 34.
20 C. S. Leasure, *Ph.D. Thesis*, New Mexico State University, Las Cruces, NM, May 1986.
21 R. L. Eatherton, *Ph.D. Thesis*, Washington State University, Pullman, WA, December 1987.
22 M. A. Baim, R. L. Eatherton and H. H. Hill, Jr., *Anal. Chem.*, 55 (1983) 1761.
23 G. A. Eiceman and V. J. Vandiver, *Anal. Chem.*, 58 (1986) 2335.
24 D. M. Lubman and M. L. Kronick, *Anal. Chem.*, 54 (1982) 1546.
25 D. M. Lubman and M. L. Kronick, *Anal. Chem.*, 54 (1982) 2289.
26 D. M. Lubman and M. L. Kronick, *Anal. Chem.*, 55 (1983) 1486.
27 R. F. D. Bradshaw, *UK Pat.*, 1 606 926 (1978).
28 C. B. Shumate and H. H. Hill, Jr., *Anal. Chem.*, 61 (1989) 601.
29 L. M. Rangarajan and G. K. Bhide, *Vacuum*, 30 (1980) 515.
30 G. S. Hurst, L. B. O'Kelly, E. B. Wagner and J. A. Stockdale, *J. Chem. Phys.*, 39 (1963) 1341.
31 J. L. Pack and A. V. Phelps, *Phys. Rev.*, 121 (1961) 798.
32 J. L. Moruzzi and A. V. Phelps, *Rev. Sci. Instr.*, 40 (1969) 461.
33 J. L. Moruzzi, *Rev. Sci. Instr.*, 38 (1967) 1284.
34 J. L. Moruzzi, J. W. Ekin, Jr. and A. V. Phelps, *J. Chem. Phys.*, 48 (1968) 3070.
35 J. Dutton, A. Goodings, A. L. K. Lucas and A. W. Williams, *J. Phys. E: Sci. Instrum.*, 21 (1988) 264.
36 Y. Gosho and A. Harada, *J. Phys. D: Appl. Phys.*, 16 (1983) 1159.
37 R. Fox and A. V. Phelps, *US Pat.*, 3 211 996 (1965).
38 J. E. Lovelock and A. Jenkins, *UK Pat.*, 1 553 071 (1975).
39 R. J. Wernlund, *US Pat.*, 3 626 181 (1971).
40 M. J. Cohen and R. W. Crowe, *US Pat.*, 3 742 213 (1973).
41 P. G. Simmonds, *J. Chromatogr.*, 399 (1987) 149.
42 J. C. Sternberg and D. T. L. Jones, *US Pat.*, 3 238 367 (1966).
43 G. E. Spangler and C. E. Collins, *Anal. Chem.*, 47 (1975) 403.
44 R. Phillips, *Sources and Applications of Ultraviolet Radiation*, Academic Press, London, 1983.
45 E. A. Mason, in T. Carr (Editor), *Plasma Chromatography*, Plenum Press, New York, 1984, p. 84.
46 L. G. Christophorou, *Electron Molecule Interaction and Their Applications*, Academic Press, London, 1984, p. 583.
47 L. G. Christophorou, *Electron Molecule Interaction and Their Applications*, Academic Press, London, 1984, p. 133.
48 A. R. Curtis and W. P. Sweetenham, *Facsimile/CHEKMAT User's Manual*, AERE Harwell, Report R12805, February 1988.
49 H. Shimamori and Y. Hatano, *J. Chem. Phys.*, 21 (1977) 187.
50 H. Shimamori and Y. Hatano, *J. Chem. Phys.*, 12 (1976) 439.
51 B. G. Young, A. W. Johnson and J. A. Garruthors, *Can. J. Phys.*, 41 (1963) 625.
52 J. L. Pack and A. V. Phelps, *J. Chem. Phys.*, 44 (1966) 1870.
53 F. Koike, *J. Phys. Soc. Jpn.*, 35 (1973) 1166.
54 F. Koike, *J. Phys. Soc. Jpn.*, 39 (1975) 1590.
55 W. T. Naff, C. D. Cooper and R. N. Compton, *J. Chem. Phys.*, 49 (1968) 2784.
56 E. P. Grimsrud and R. G. Stebbins, *J. Chromatogr.*, 155 (1978) 19.
57 D. R. Bates, *Adv. Atom. Mol. Phys.*, 20 (1985) 1.
58 B. H. Mahan, *Adv. Chem. Phys.*, 23 (1973) 1.
59 V. J. Vandiver, *Ph.D. Thesis*, New Mexico State University, Las Cruces, NM, May 1987.
60 R. N. Snuggs, D. J. Volz, J. E. Schummers, C. W. Martin and E. W. McDaniel, *Phys. Rev.*, A3 (1971) 477.